An Analytical Model for the Tension-Shear Coupling of Woven Fabrics with Different Weave Patterns under Large Shear Deformation

Yanchao Wang [1,2,3,*]**, Weizhao Zhang** [4]**, Huaqing Ren** [5]**, Zhengming Huang** [2]**, Furong Geng** [1]**, Yongxiang Li** [1] **and Zengyu Zhu** [6]

[1] Research & Design Center, Guangzhou Automobile Group Co. Ltd., Guangzhou 511434, China; gengfurong@gacrnd.com (F.G.); liyongxiang@gacrnd.com (Y.L.)

[2] School of Aerospace Engineering & Applied Mechanics, Tongji University, Shanghai 200092, China; huangzm@tongji.edu.cn

[3] School of Mechanical and Automotive Engineering, South China University of Technology, Guangzhou 510006, China

[4] Department of Mechanical and Automation Engineering, Chinese University of Hong Kong, Hong Kong, China; weizhaozhang2014@u.northwestern.edu

[5] Department of Mechanical Engineering, Northwestern University, Evanston, IL 60208, USA; huaqingren2013@u.northwestern.edu

[6] Guangdong Yatai New Material Technology Co. Ltd, Sihui City 526241, China; ceo@ytbxg.com

* Correspondence: wangyanchao@gacrnd.com

Featured Application: The work provides an analytical model which can be useful in the optimization of process parameters of dry fabrics in material-forming industries.

Abstract: It is essential to accurately describe the large shear behavior of woven fabrics in the composite preforming process. An analytical model is proposed to describe the shear behavior of fabrics with different weave patterns, in which tension-shear coupling is considered. The coupling is involved in two parts, the friction between overlapped yarns and the in-plane transverse compression between two parallel yarns. By introducing the concept of inflection points of a yarn, the model is applicable for fabrics with different weave patterns. The analytical model is validated by biaxial tension-shear experiments. A parametric study is conducted to investigate the effects of external load, yarn geometry, and weave structure on the large shear behavior of fabrics. The developed model can reveal the physical mechanism of tension-shear coupling of woven fabrics. Moreover, the model has a high computational efficiency due to its explicit expressions, thus benefiting the material design process.

Keywords: analytical model; fabrics; weave pattern; shear deformation; tension-shear coupling

1. Introduction

Woven fabrics and their composites have been widely used in engineering due to the outstanding mechanical performance [1,2]. Recently, wet compression molding of woven composites has attracted more attention because of its high efficiency in the manufacturing process [3]. The shear deformation, the dominant mode of a woven fabric in the forming process, is closely related to the yarn reorientation which is critical for the mechanical properties of a composite. It is noted that a blank holder is commonly used to provide a tensile force in a preforming process so that wrinkle onset can be postponed [4]. Moreover, the shear stiffness of a woven fabric can be significantly affected by applying a tensile force

along yarns [5,6]. Thus, it is critical to establish a model that can account for tension-shear coupling for the large shear deformation of a woven fabric.

Approaches to investigate the shear behavior of a woven fabric can be classified into three categories [7]: experimental testing, numerical simulation, and analytical modeling. In the first category, many kinds of experimental configurations have been reported [8,9]. For the second category, numerical simulations of woven fabrics have also been widely investigated, for example, Boisse et al. [10], Zhang et al. [11], and Erol et al. [12]. Experiments are essential for the understanding of mechanical properties of materials. However, it is too expensive to obtain all the properties of a material under various load cases only upon experiments. Conversely, numerical simulations and analytical models can predict mechanical behaviors of a material based on some basic test results, which significantly accelerates the application process of a material. Furthermore, compared with numerical methods, analytical models are superior in computational efficiency and understanding of physical mechanism. Thus, this work mainly focuses on analytical models.

Analytical models for shear behavior of woven fabrics can be split into two categories: kinematic models and mechanical models. The kinematic models [13,14] are succinct, but they cannot account for the effect of mechanical behaviors of yarns on the deformation of woven fabrics. To tackle this problem, mechanical models were developed. Mechanical models can be roughly divided into two families: continuum models and discrete models. With respect to the former family, King et al. [15] proposed a continuum mechanics model for woven fabrics, where the bending, tension, and shear behaviors of yarns are modeled by virtual springs. The parameters of the virtual springs are obtained from experiments directly, meaning that the coupling between tension and shear properties is only involved implicitly. Peng et al. [16] developed a continuum material model for woven fabrics, where the shear and tension stresses are decoupled by using a non-orthogonal coordinate system. However, the interaction between shear and tension properties still exists but is not considered. Gong et al. [17] proposed an anisotropic hyper-elastic model for the preforming process of woven fabrics, where the tension-shear coupling effect was studied. Nevertheless, the coupling factors are directly obtained by fitting experimental data, meaning that the coupling mechanism is not fully revealed.

In the range of discrete models, Lomov and Verpoest [18] presented an analytical model to investigate the tension-shear coupling in woven fabrics. In their work, the effect of transverse in-plane compression of yarns on the shear property is considered indirectly by the friction dissipation energy, which may underestimate its contribution. Zhu et al. [19] pointed out that the shear dissipation energy can be divided into three parts: yarn sliding, yarn compression, and yarn rotation. However, no tensile forces along yarns were studied in the work of Zhu et al. [19]. Erol et al. [20] gave analytical expressions for the tensile, compressive, and shear properties of woven fabrics by treating the structure as a system of beams and springs. Similarly, Nasri et al. [21] developed a hybrid discrete hypo-elastic model for woven fabrics, where the tensile and shear properties are modeled by tensile and torsional springs, respectively. The simulation results of both Erol et al. [20] and Nasri et al. [21] agree well with experimental data. However, in their work, the constitutive equations for the mechanical properties of woven materials are given by curve-fitted exponential or polynomial functions. Such operations are inconvenient when the weave pattern changes with design requirements.

To the authors' knowledge, the tension-shear coupling related parameters in most models must be determined by fitting experimental data, thereby needing to redo experiments when the weave pattern changes. In this work, an analytical approach is proposed to model the large shear deformation of woven fabrics. The tension-shear coupling mechanism is explicitly revealed by the friction dissipation energy and transverse compression dissipation energy. In addition, the effect of the weave pattern on the shear behavior of a fabric is considered by introducing the number of yarn inflection points. Thus, the model is applicable for fabrics with different weave patterns without more experiments required.

2. Tension-Shear Coupling Model

2.1. Geometrical Model

Figure 1 shows the configuration of a plain-woven representative volume element (RVE). The RVE geometric parameters, w_0, g_0, and N_y, are, respectively, the yarn width, the yarn gap, and the yarn amount in the RVE. L_R, the side length of the RVE, is defined as follows:

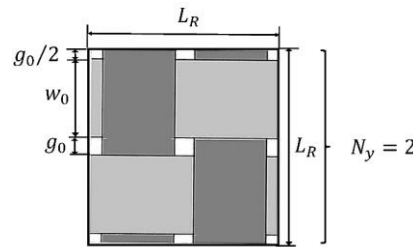$$L_R = N_y(w_0 + g_0). \tag{1}$$

Figure 1. Geometry of a plain-woven RVE.

In order to focus on the tension-shear coupling, this work only considers the case that the warp and fill yarns have identical geometry. It should be noted that Equation (1) is applicable for fabrics with different weave patterns. The plain weave pattern shown in Figure 1 is only an example for illustration.

The number of inflection points of a yarn, η_y is introduced to characterize different weave patterns. In a woven fabric, a warp yarn passes over and under fill yarns in sequence, and vice versa. The ratio of the under and over areas of warp and fill yarns determines the weave pattern. In this work, when a yarn turns from under to over or from over to under one time, it is counted as one inflection point. The inflection point at the boundary of an RVE is counted as a half point. For example, as shown in Figure 2a, the inflection point number of a warp yarn is 2. The weave pattern of RVEs with the same yarn amounts can be distinguished by different yarn inflection point numbers. For example, as shown in Figure 2a,b, both the twill and plain RVEs have 4 warp and 4 fill yarns, but their inflection point numbers of the warp yarn are 2 and 4, respectively. The number of inflection points in an RVE determines the normal pressure between overlapped yarns induced by the tensile force. Furthermore, normal pressure is closely related to the tension-shear coupling which will be explained in detail hereinafter. Hence, it is believed that the inflection point number is critical to evaluate the effects of different weave patterns on the tension-shear coupling of fabrics.
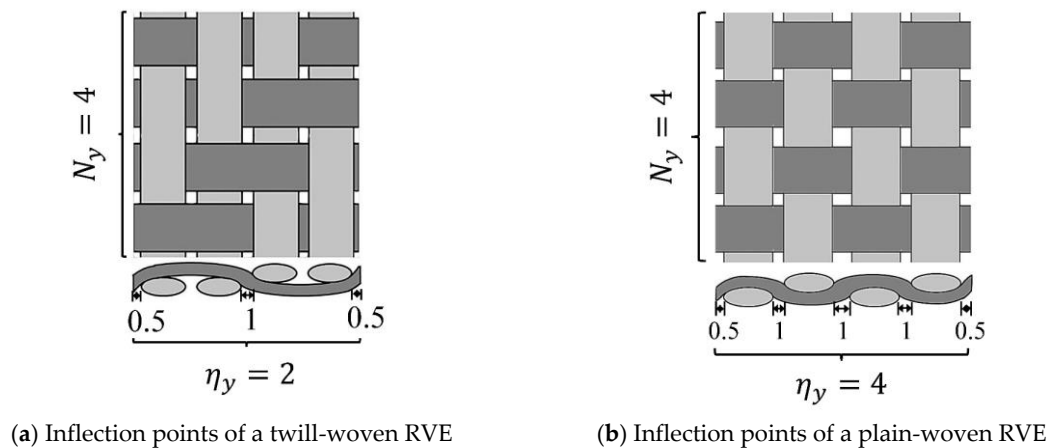

(**a**) Inflection points of a twill-woven RVE

(**b**) Inflection points of a plain-woven RVE

Figure 2. Illustration of inflection points.

2.2. Incremental Energy Equilibrium Theory

In forming manufacturing industries, the shape and stress state of a formed fabric depend on the forming process parameters, such as molding shape, forming rate, etc. Numerical simulations are generally used to optimize such forming process parameters. The key to such a simulation is a reliable constitutive relation that describes the mechanical behavior of an RVE of a fabric. In practice, blank-holders are often used to introduce tension forces along yarns so that the wrinkling phenomenon may be postponed. Besides, a fabric is majorly shear deformed in the forming process. Thus, it is critical to establish a constitutive relation for large shear deformation of a fabric RVE with the consideration of tension-shear coupling. Once the constitutive relationship is obtained, the numerical simulation can be realized subsequently. Thus, this work mainly investigates a fabric RVE subjected to a combined tension and shear load, as shown in Figure 3.
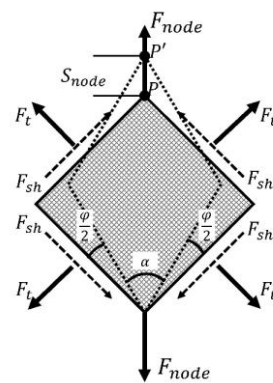

Figure 3. Shear deformation of a fabric RVE.

The RVE is applicable for different weave patterns. Thus, no specific weave pattern is illustrated in Figure 3. The RVE is firstly subjected to tension loads along yarns, F_t. The tension forces remain constant throughout the load case. Then, the RVE undergoes shear deformation under the force F_{node} at the node P of the RVE. The node P moves to P' due to the shear deformation. The shear force F_{sh} is the projection of F_{node} to the boundary of the RVE. The relationship between F_{sh} and F_{node} is given as follows:

$$F_{sh} = \frac{F_{node}}{2cos\left(\frac{\pi}{4} - \frac{\varphi}{2}\right)}. \tag{2}$$

As mentioned in the above paragraph, the tension forces along yarns are applied before the shear deformation, meaning that a yarn has been stretched before the RVE is sheared. Thus, no tension input energy is involved in the shear deformation. The input energy generated by the node force F_{node} will be dissipated by friction, transverse compression, thickness variation, yarn elongation, yarn sliding, and waviness angle variation. Among these dissipation energies, the former two are dominant. The yarn thickness may increase due to in-plane transverse compression, but the variation is small since the increase of yarn thickness will be restricted by overlapped yarns. The yarn elongation is negligible, since the longitudinal modulus of a yarn is much larger than the shear and transverse compressive properties of a fabric. The yarn sliding is also negligible, since a couple of balanced tension forces are applied to the end of a yarn. The waviness angle variation mainly results from yarn sliding and thickness variation, thereby also being insignificant. Thus, only the friction and transverse compression dissipation energies are considered. According to the energy equilibrium theory, the input energy should equal the sum of the dissipation energies. Hence, the following equation is obtained:

$$dW_{node} = dW_{fri} + dW_{com}, \tag{3}$$

where $\mathrm{d}W_{node}$ is the input energy increment generated by the node force, F_{node}. $\mathrm{d}W_{fri}$ and $\mathrm{d}W_{com}$ are incremental energy dissipated by the respective friction and transverse compression of yarns.

Our goal is to express all items in Equation (3) as functions of shear force, shear angle, geometric parameters, and mechanical properties of yarns so that a shear stress-angle curve can be obtained eventually.

2.3. Input Energy of Shear Force

As shown in Figure 3, when a fabric RVE undergoes shear deformation, the node P moves to P' with displacement of S_{node}. The yarn angle α decreases with the increase of shear angle φ, where a relation exists: $\alpha = \pi/2 - \varphi$. Then, the incremental input energy is given by

$$dW_{node} = F_{node}dS_{node}. \tag{4}$$

In order to characterize the shear behavior of the RVE, it is necessary to express F_{node} and dS_{node} as functions of the shear stress and shear angle. Firstly, with Equation (2), the following equation is given as:

$$F_{node} = 2cos\left(\frac{\pi}{4} - \frac{\varphi}{2}\right)F_{sh}. \tag{5}$$

Furthermore, for the purpose of normalization, the shear stress τ_{sh} instead of the shear force F_{sh} is employed. Then, we have

$$F_{sh} = 2\tau_{sh}L_R t, \tag{6}$$

where L_R is the side length of the RVE, and t is the yarn thickness. Secondly, dS_{node} is the differentiation of the node displacement S_{node}, whose relationship is given by

$$dS_{node} = \frac{d(S_{node})}{d\varphi}d\varphi. \tag{7}$$

From Figure 3, S_{node} is given by

$$S_{node} = 2L_R \cos\left(\frac{\pi}{4} - \frac{\varphi}{2}\right) - 2L_R cos\frac{\pi}{4}. \tag{8}$$

Then, dS_{node} is given by

$$dS_{node} = \frac{d(S_{node})}{d\varphi}d\varphi = L_R sin\left(\frac{\pi}{4} - \frac{\varphi}{2}\right)d\varphi. \tag{9}$$

Finally, substituting Equations (5), (6), and (9) into Equation (4), the input energy is expressed in terms of the shear stress and the geometric parameters as follows:

$$dW_{node} = 4tL_R^2\tau_{sh}\cos\left(\frac{\pi}{4} - \frac{\varphi}{2}\right)sin\left(\frac{\pi}{4} - \frac{\varphi}{2}\right)d\varphi = 2tL_R^2\tau_{sh}sin\left(\frac{\pi}{2} - \varphi\right)d\varphi = 2tL_R^2\tau_{sh}cos\varphi d\varphi. \tag{10}$$

2.4. Dissipation Energy of Friction

Figure 4a is a crossover point of two yarns. As shown in Figure 4b, a friction force is generated when a yarn rotates. An equivalent circle is used to approximate the contact area of overlapped yarns. It is reasonable to assume that the friction force is evenly distributed in the contact area. Imagine an infinitesimal sector whose side lengths are dr and $rd\phi$, as shown in Figure 4c. The sector moves from A to A' with the yarn rotation. Then, the moment of the friction force to the point O is given by

$$M_{fri} = \int_0^{2\pi} \int_0^R \frac{F_{fri}}{\pi R^2} r \cdot r dr d\phi = \frac{2}{3}F_{fri}R. \tag{11}$$

(**a**) Cross point in an RVE

(**b**) Illustration of friction force

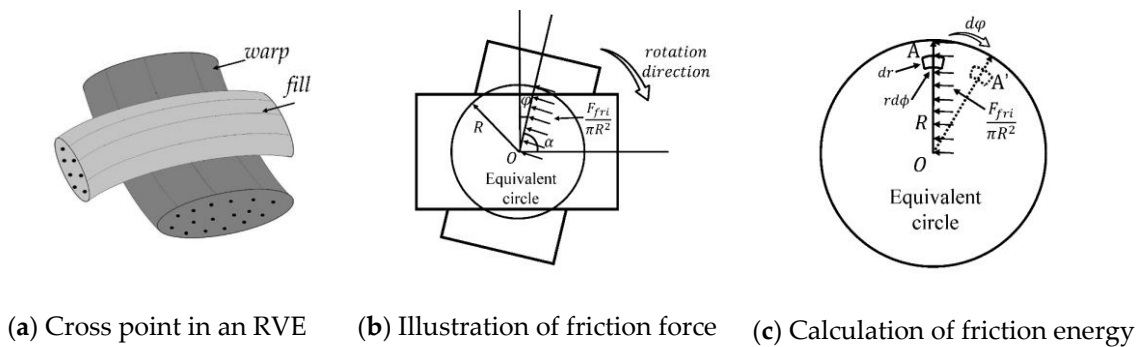(**c**) Calculation of friction energy

Figure 4. Dissipation energy of friction.

Furthermore, the friction dissipation energy in an RVE is obtained as

$$dW_{fri} = N_y^2 M_{fri} d\varphi = \frac{2}{3} N_y^2 F_{fri} R \mathrm{d}\varphi, \tag{12}$$

where R is the equivalent radius. The contact area varies with the shear angle until parallel yarns contact each other in in-plane transverse direction. Thus, R is expressed as

$$R = \begin{cases} \frac{w_0}{\sqrt{\pi \cos\varphi}} & \varphi < \varphi_L \\ \frac{w_0}{\sqrt{\pi \cos\varphi_L}} & \varphi \geq \varphi_L \end{cases}, \tag{13}$$

where φ_L is the shear-locking angle, meaning that parallel yarns start to contact each other in in-plane transverse direction. The shear-locking angle can be expressed as

$$\cos\varphi_L = \frac{w_0}{w_0 + g_0}. \tag{14}$$

It should be noted that the shear angle keeps increasing after φ_L due to in-plane transverse compression of yarns. In other words, the shear angle is actually not locked. However, following the nomenclature of textile forming, the shear-locking angle is still employed.

For simplicity, Coulomb's friction theory is employed. Before a yarn rotates, the static friction force can be approximately seen as linearly dependent on the shear angle. When a yarn rotates, the friction force F_{fri} is calculated from the friction factor μ and the contact force between overlapped yarns F_c. The friction force is expressed as:

$$F_{fri} = \begin{cases} \frac{\varphi}{\varphi_0} \mu F_c & \varphi < \varphi_0 \\ \mu F_c & \varphi \geq \varphi_0 \end{cases}, \tag{15}$$

where φ_0 is the critical shear angle when a yarn starts to rotate. Obviously, the friction force depends on the contact force between overlapped yarns, F_c. F_c consists of two parts: the one induced by the tension force along a yarn, F_t^c, and the initial contact force induced by the yarn bending, F_0^c, as shown in the following equation:

$$F_c = F_t^c + F_0^c. \tag{16}$$

Ideally, F_0^c should be calculated from the yarn bending stiffness and the bending angle. However, the measured bending stiffness has large scatter, and its value is sensitive to the load status of a yarn. Thus, it is better to curve-fit F_0^c by comparing prediction results to experimental data.

Figure 5 illustrates the contact force induced by the tension force along a yarn for a plain-woven fabric. θ is the waviness angle of a yarn. L_{in} is the length of the inflected part of a yarn. Then, F_t^c is:

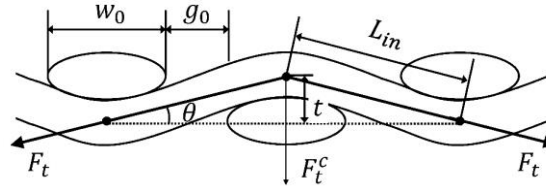$$F_t^c = 2F_t sin\theta = 2F_t \frac{t}{L_{in}} = \frac{2tF_t}{\sqrt{(w_0 + g_0)^2 + t^2}}. \tag{17}$$

Figure 5. The contact force produced by the tension force of a yarn (plain-woven fabric).

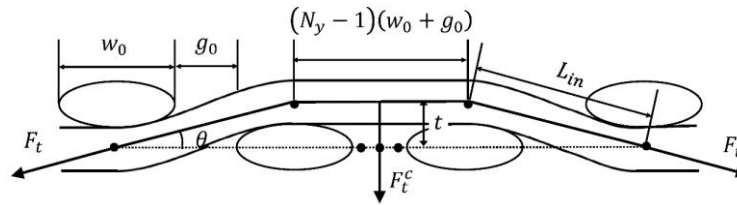For fabrics with different weave patterns, the illustration of the contact force is shown in Figure 6.

Figure 6. The contact force produced by the tension force of a yarn (different weave pattern).

Then, the contact force at one cross point is:

$$F_t^c = \frac{2\eta F_t sin\theta}{N_y} = \frac{2\eta_y t F_t}{N_y \sqrt{(w_0 + g_0)^2 + t^2}}. \tag{18}$$

The friction force can be calculated by substituting Equation (18) into Equation (16) and then into Equation (15).

Finally, the dissipation energy, dW_{fri}, is obtained by substituting Equations (15) and (13) into Equation (12). The expression of dW_{fri} is obtained:

$$dW_{fri} = \begin{cases} \frac{2}{3}N_y^2 \frac{\varphi}{\varphi_0}\mu\left(\frac{2\eta_y t F_t}{N_y\sqrt{(w_0+g_0)^2+t^2}} + F_0^c\right)Rd\varphi & \varphi < \varphi_0 \\ \frac{2}{3}N_y^2\mu\left(\frac{2\eta_y t F_t}{N_y\sqrt{(w_0+g_0)^2+t^2}} + F_0^c\right)Rd\varphi & \varphi \geq \varphi_0 \end{cases} \tag{19}$$

2.5. Dissipation Energy of in-plane Transverse Compression

As shown in Figure 7a, parallel yarns start to contact each other at the shear-locking angle. As the shear angle increases, the yarns are transversely compressed under the in-plane transverse compression force F_{com}. The points C and D move to C' and D', and the total width reduction of a yarn is Δw, as illustrated in Figure 7b. Since no yarn sliding is considered in this work, the side length of the parallelogram ABCD remains constant, which is $(w_0 + g_0)$.
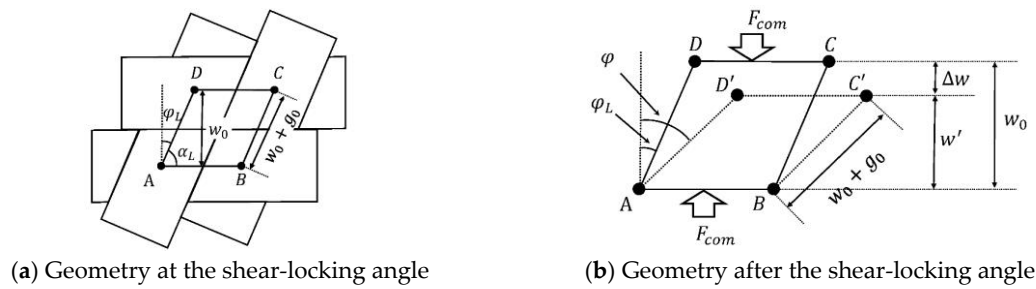
(**a**) Geometry at the shear-locking angle   (**b**) Geometry after the shear-locking angle

Figure 7. In-plane transverse compression of an RVE.

In an infinitesimal load increment, F_{com} can be seen as constant. Since the fill and warp yarns are consistent in geometry and mechanical properties, the dissipation energy of the in-plane transverse compression of a fabric RVE is

$$\mathrm{d}W_{com} = 2N_y^2 F_{com} dw, \tag{20}$$

where dw is the differentiation of Δw. Δw and dw are given by

$$\Delta w = w_0 \varepsilon_{com}, \tag{21}$$

$$dw = w_0 d\varepsilon_{com}, \tag{22}$$

where ε_{com} is the in-plane transverse compressive strain of a yarn. From the view point of simplicity, it is reasonable to assume that the yarn compression is linear. Then, the compression force F_{com} is calculated with the following equation:

$$F_{com} = t(w_0 + g_0)E_{com}\varepsilon_{com}, \tag{23}$$

where E_{com} is the transverse compressive modulus of a yarn.

Please remember that our goal is to obtain the constitutive relation between the shear stress and shear angle of a fabric RVE. Thus, ε_{com} must be written as a function of the shear angle. φ_L is the shear-locking angle given by Equation (14). Obviously, when $\varphi \leq \varphi_L$, the width is not compressed, and both ε_{com} and $d\varepsilon_{com}$ are zero. When $\varphi > \varphi_L$, is the following equation is given as:

$$\Delta w = w_0 - w' = (w_0 + g_0)(cos\varphi_L - cos\varphi), \quad \varphi > \varphi_L. \tag{24}$$

Then, ε_{com} is obtained as

$$\varepsilon_{com} = \frac{\Delta w}{w_0} = \frac{w_0 - w'}{w_0} = \frac{(w_0 + g_0)(cos\varphi_L - cos\varphi)}{w_0}, \quad \varphi > \varphi_L. \tag{25}$$

Furthermore, $d\varepsilon_{com}$ is reached:

$$d\varepsilon_{com} = \frac{d(\varepsilon_{com})}{d\varphi}\mathrm{d}\varphi = \frac{(w_0 + g_0)sin\varphi}{w_0}d\varphi, \varphi > \varphi_L. \tag{26}$$

Obviously, when $\varphi \leq \varphi_L$, the dissipation energy is zero. When $\varphi > \varphi_L$, $\mathrm{d}W_{com}$ can be achieved by substituting Equations (25) and (26) into Equations (22) and (23) and then into Equation (20). Finally, the expression of $\mathrm{d}W_{com}$ is achieved:

$$\mathrm{d}W_{com} = 2N_y^2 E_{com} \frac{t(w_0 + g_0)^3}{w_0}(cos\varphi_L - cos\varphi)sin\varphi d\varphi, \quad \varphi > \varphi_L. \tag{27}$$

2.6. Model Summary

Both the input energy and dissipation energies of friction and transverse compression are expressed as functions of the shear stress and shear angle. Then, the relation between shear stress and shear angle can be obtained by solving the energy equilibrium, Equation (3). It is noted that the friction dissipation energy is sensitive to the number of inflection points in an RVE, indicating that the present model can consider the effect of different weave patterns on the shear deformation of fabrics. In addition, the tension-shear coupling mechanism appears from two aspects in the present model. Firstly, the effect of tension force on the shear property of a fabric is directly reflected by the shear friction dissipation energy. An increase in the tension force leads to the increase of contact force between overlapped yarns and then results in the increase of friction dissipation energy. Obviously, a larger dissipation energy means larger resistance in deformation. Secondly, the tension force will make a yarn shrink. Generally, the transverse compressive modulus will rise due to the shrinking effect. Furthermore, the increase of transverse compressive modulus also generates more dissipation energy. With the help of the analytical model developed in this work, the effect of tension on the shear behavior of fabrics can be analyzed explicitly.

3. Model Validation

In this part, the present model is validated by experimental results of a dry woven fabric under tension and shear loads. The experimental data for a carbon fiber plain-woven fabric subjected to biaxial tension and shear force were presented in Nosrat-Nezami et al. [22]. As shown in Figure 8, the experiment is constructed by adding a tensile device to a picture frame configuration, and a needle bar is set up between clamps to guarantee the free rotation of yarns. The geometric information of the test specimen is shown in Table 1. The friction factor between warp and fill yarns of a carbon fabric is 0.6 according to Najjar et al. [23] and Allaoui et al. [24]. Please note that the width and gap of warp and fill yarns are slightly different. The shear-locking angle is determined by geometry of the yarn family which is first in-plane transversely contacted. Thus, the width and gap of the fill yarn are used in the present model.
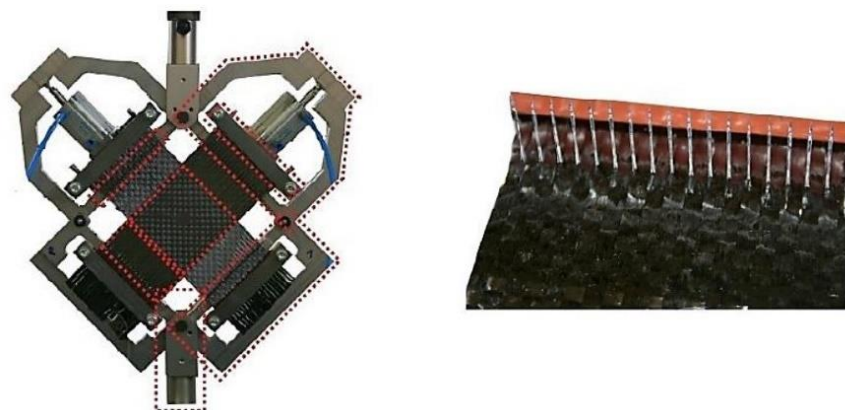

Figure 8. Biaxial tension and shear test on a plain-woven carbon fabric [22].

Table 1. Geometric information of the T700-12K carbon fiber plain-woven fabric specimen [22].

Specimen Size	Fabric Thickness	Warp Width	Warp Gap	Fill Width	Fill Gap
100 × 100 mm	0.45 mm	4.11 mm	0.78 mm	4.94 mm	0 mm

When a tensile force is applied to a yarn, due to the yarn shrinking and the out-of-plane compression between overlapped yarns, the fabric thickness decreases and the transverse compressive modulus of the yarn increases. However, the variations of thickness and transverse compressive

modulus are difficult to be measured experimentally. According to the thickness-pressure relation shown in Figure 9, Ivanov and Lomov [25] suggested that the thickness variation and the transverse compressive of a yarn can be approximated as bilinear functions of the compressive force. Please note that, although a fabric is subjected to a tension force along the yarn direction, the yarn is actually compressed in the transverse direction due to the yarn shrinking and the out-of-plane compression between overlapped yarns. Thus, the transverse stress state of a yarn in this work is similar to the transvers compressive test shown in the work of Ivanov and Lomov [25]. Besides, the materials involved in Figures 8 and 9 are both carbon fabrics with a 12 K yarn bundle. Thus, the quasi-bilinear trend shown in Figure 9 is reasonably applicable for the validation in this work.
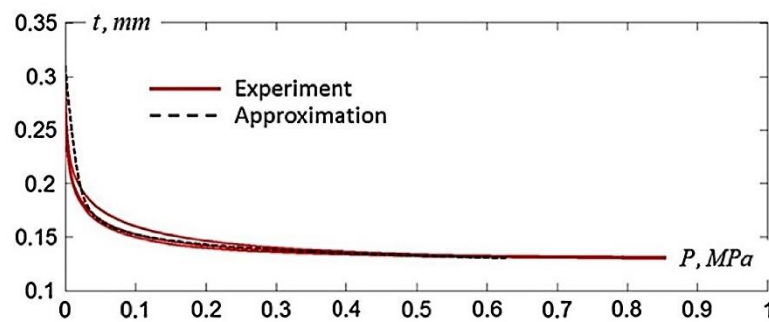

Figure 9. Thickness-compressive pressure of a dry carbon yarn [23].

For the cases in Nosrat-Nezami et al. [22], the maximum tensile load is 2.4 N/mm. If the contact force induced by yarn bending is ignored, the tensile load of 2.4 N/mm corresponds to a compressive pressure of about 0.05 MPa, according to Equations (16) and (18), which is located around the first linear segment in Figure 9. Thus, it is rational to assume that the thickness and transverse compressive moduli linearly vary with the tensile force. In addition, the bending stiffness also varies due to the yarn shrinking. Furthermore, the bending stiffness directly affects the initial contact force F_0^c induced by yarn waviness. Thus, it is also reasonable to set F_0^c as a linear function of the tension force. Then, the thickness t, the compressive modulus E_{com}, and the initial contact force F_0^c can be obtained by a linear curve-fitting process from the cases of no tension and 2.4N/mm tension. Besides, the shear angle when a yarn starts to rotate, φ_0, can be approximately seen as a constant throughout the load process, since it is not sensitive to the contact force between overlapped yarns. Thus, one curve is enough to fit the φ_0. Overall, the cases of no tension and 2.4 N/mm tension are employed to curve-fit model parameters, and the other cases are used for validation. All the curve-fitted parameters are shown in Table 2.

Table 2. Curve-fitting parameters for a carbon fiber plain-woven fabric.

Loading Cases	No Tension	0.8 N/mm	1.6 N/mm	2.4 N/mm
φ_0 (°)	1.5°	1.5°	1.5°	1.5°
F_0^c (N)	0.2	0.33	0.47	0.6
t (mm)	t	0.86 t	0.73 t	0.6 t
E_{com} (MPa)	0.25	0.83	1.41	2

Figure 10 compares the results of the present model and experimental data. The cases of no tension and 2.4 N/mm tension are used to curve-fit the parameters of the present model, t, φ_0, F_0^c, and E_{com}. The cases of 0.8 N/mm and 1.6 N/mm are used for validation. Equation (28) provides a method to quantitatively characterize the average error between experimental data and the predicted results.

$$\text{Err} = \sum_{i=1}^{M} \frac{1}{M} \frac{\sqrt{\left(\tau_{sh}^{pr}(\varphi_i) - \tau_{sh}^{ex}(\varphi_i)\right)^2}}{\tau_{sh}^{ex}(\varphi_i)}, \tag{28}$$

where φ_i is the evenly distributed shear angle point with an angle-interval of around 5°. $\tau_{sh}^{pr}(\varphi_i)$ and $\tau_{sh}^{ex}(\varphi_i)$ are the corresponding predicted and measured shear stresses for each φ_i. M is the number of collected data points of a curve. The average errors for the four load cases are shown in Figure 10. The average errors of the four cases are around 10%, which is good enough considering the scatter of measured data.
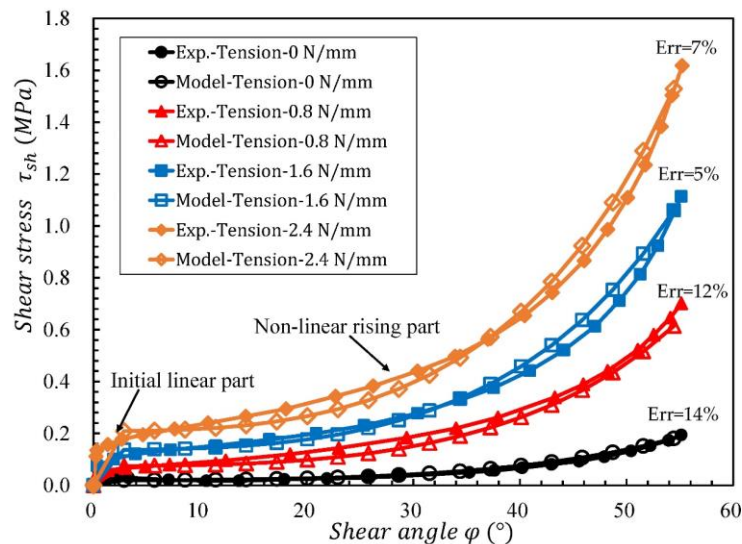

Figure 10. Comparison between the analytical model and experimental data of a carbon plain-woven fabric under bi-axial tension and shear load.

For the no tension and 2.4 N/mm tension cases, the theoretical curves agree well with experimental results, proving that the present model can effectively describe the shear mechanism and the tension-shear coupling effect of fabrics under biaxial tension. For the cases of 0.8 N/mm and 1.6 N/mm, the deviations between predicted and experimental results are very small, verifying the prediction capability of the present model.

Comparing the curves of the four cases, it is found that the shear rigidity of a fabric significantly increases with the applied tension force. Thus, it is evident that the tension-shear coupling must be taken into account in the material forming process of fabrics. As shown in Figure 10, a stress-strain curve can be divided into two parts: the initial linear part and the nonlinear part. The initial part is induced by the static friction between overlapped yarns before a yarn rotates. The maximum value of the static friction force determines the initial shear stress value of the nonlinear part. A higher tension force leads to a larger maximum static friction force, thereby resulting in stiffer shear property of a fabric. Thus, the friction between overlapped yarns is one source of the tension-shear coupling. For the nonlinear part, the stiffness rapidly increases when the tension force varies from zero to 2.4 N/mm. This happens because the fiber density of a yarn becomes larger due to yarn shrinking induced by a tension force. A higher fiber density means a higher transverse compressive Young's modulus. Furthermore, higher transverse stiffness of yarns brings a larger shear resistance for the shear deformation of fabrics. Obviously, the transverse compression of yarns is one main source of the tension-shear coupling.

For general fabrics, there should be a flat part between the initial linear part and the nonlinear rising part. The flat part is induced by friction during shear deformation before transverse compression of parallel yarns occurs. However, the fill gap is zero for the case in Figure 10, meaning that parallel yarns contact each other when a yarn starts to rotate. Thus, no obvious flat part is observed in Figure 10.

4. Parametric Study

It is essential to understand the effect of geometry and mechanical properties of yarns on the large shear behavior. In this work, a kind of carbon fiber woven fabric is taken as an example. It should

be noted in Figure 10 that the unit of tension force along a yarn is N/mm, meaning that the force is homogenized by the side length of an RVE. Thus, the force along a yarn is dependent on the thickness of a fabric. Conversely, the parametric study requires that the tensile load is independent of thickness variation. Thus, a tensile stress σ_y with unit of MPa is used. As a reference, some basic parameters are reasonably set in Table 3. The sensitivity study is performed by varying one of these parameters while keeping the others constant.

Table 3. Parameter values of a reference-woven fabric.

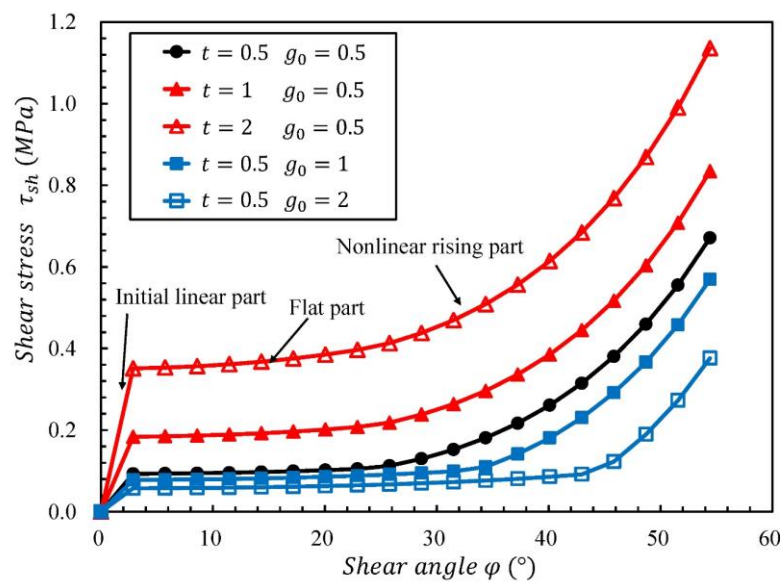| Parameters	Value	Parameters	Value
Weave pattern	plain	Initial shear angle φ_0	2°
Yarn width w_f & w_w	5 mm	Tension stress along yarns σ_y	5 MPa
Yarn gap g_f & g_w	0.5 mm	Friction factor μ	0.6
Yarn thickness t_f & t_w	0.5 mm	Compressive modulus of yarn E_{com}	1 MPa

Figure 11a shows the shear deformation curves of fabrics with different weave patterns. The weave pattern is characterized by η_y/N_y, the ratio between the inflection points of a yarn and the number of yarns in an RVE. The ratios are 1, 1/2, and 1/4 for plain woven, 2*2 twill, and 8 harness satin, respectively. As shown in Figure 11a, a higher ratio corresponds to a higher shear stiffness. The result is reasonable because a higher ratio means more interaction between fill and warp yarns.

Figure 11b is the parametric study of the fabric geometry. It is found that the shear stiffness increases with the increase of yarn thickness but decreases with the increase of yarn gap. This is because the waviness angle becomes larger when a yarn becomes thicker. Thus, the contact force between overlapped yarns increases, though the tension force along the yarn remains unchanged. However, the increase of yarn gap reduces the waviness angle, thereby weakening the effect of the tension force on shear deformation. Besides, the shear-locking phenomenon is postponed with the increase of gap size, 25° for $g_0 = 0.5$, 34° for $g_0 = 1$, and 44° for $g_0 = 2$. The transverse compression of parallel yarns is one main source of the shear resistance. Thus, the rising shear-locking angle significantly reduces the shear rigidity of a fabric.

Figure 11c illustrates the effect of the yarn property and the tensile load on the shear behavior of a fabric. It should be noted that in real cases, the transverse compressive modulus E_{com} is sensitive to the tensile load F_t. However, in the sensitivity study, the two parameters are assumed to be independent so as to investigate the effect of each parameter on the shear behavior. It can be seen that the increase of tensile force along yarns results in a larger shear rigidity of a fabric. Moreover, each curve in Figure 11 can be divided into three parts, the initial linear part, the flat part, and the nonlinear rising part. Curves in Figure 11a–c indicate that the weave pattern, the yarn geometry, and the tensile load along yarns can only influence the maximum stress of the first part and the shear stress of the flat part but have no effect on the third part. However, as shown in Figure 11c, the growth of E_{com} significantly increases the slope of the third part of a curve, thereby enhancing the shear rigidity of a fabric. This happens because the effects of the weave pattern, the geometry, and the tensile load on shear behavior are characterized by the friction force which controls the linear and the flat part. However, the third nonlinear rising part is mainly controlled by the transverse compression of yarns.
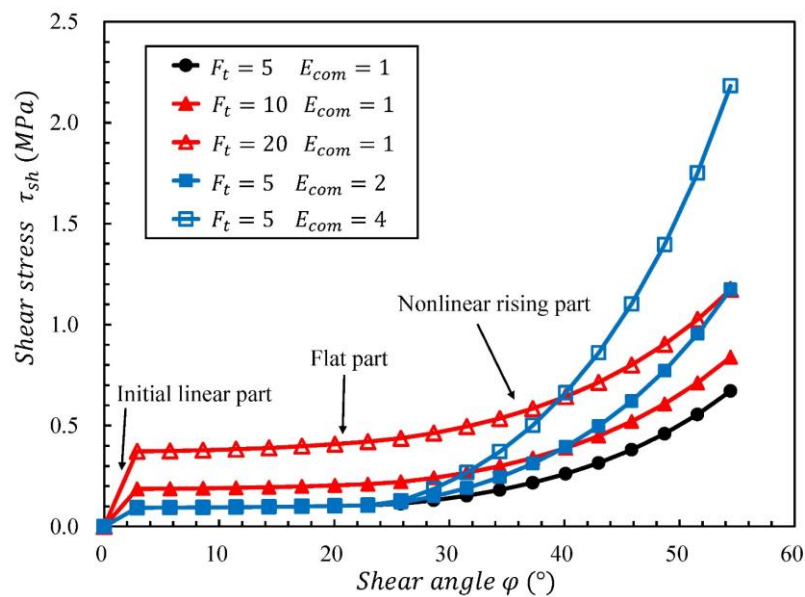
(**a**) Effect of weave pattern

(**b**) Effect of geometry of yarns

Figure 11. *Cont.*

(**c**) Effect of mechanical property and tensile load

Figure 11. Sensitivity study on the shear behavior of a fabric.

5. Conclusions

An analytical model is proposed to describe the tension-shear coupling effect of fabrics with different weave patterns under large shear deformation. Different weave patterns are characterized by the number of inflection points of yarns. In this work, the tension-shear coupling mechanism can be revealed from two aspects, the friction dissipation energy and the in-plane transverse compressive dissipation energy. On the one hand, the subjected tensile force along yarns increases the contact force between overlapped yarns, leading to the growth of the friction dissipation energy. Then, larger friction dissipation energy brings more resistance with respect to shear deformation, thereby increasing the shear rigidity of a fabric. On the other hand, the tensile load along a yarn makes the yarn shrink. The shrinking improves the transverse compressive modulus of the yarn. Besides, the transverse compressive modulus of a yarn is also improved due to the compressive force between overlapped yarns induced by the tension force. Then, the dissipation energy of the transverse compression of yarns becomes larger due to the increase of the mechanical properties of yarns, thus enhancing the shear rigidity of a fabric. In addition to the description of the tension-shear coupling mechanism, the present model has a high computational efficiency due to its explicit and analytical expressions.

The model is validated by experimental results of the shear behavior of a fabric under different biaxial tensile loads. Furthermore, parametric studies are carried out using the present model. In general, fewer inflection points, a larger gap-to-width ratio, and softer in-plane compressive moduli decrease the shear stiffness of a fabric, which can improve the formability of a fabric. When tensile force along yarns is utilized to reduce wrinkling, one should consider that the tensile force will also affect the shear property of a fabric and will further affect the yarn re-orientation. With the help of the present analytical model, engineers can easily optimize the design of fabrics with different weave patterns. Because of the high computational efficiency of the model, the optimization process can be significantly improved.

Author Contributions: Conceptualization, Y.W, Z.H., F.G., Y.L., and Z.Z.; Funding acquisition, Y.W., Z.H., and Z.Z.; Methodology, Y.W., W.Z., and H.R.; Project administration, Z.H. and Z.Z.; Supervision, Z.H., F.G, Y.L., and Z.Z.; Validation, Y.W., W.Z., and H.R.; Writing—original draft, Y.W.; Writing—review & editing, Y.W., W.Z., and H.R. All authors have read and agreed to the published version of the manuscript.

Conflicts of Interest: The authors declare no conflict of interest.

References

1. Soleimani, S.M.; Sayyar Roudsari, S. Analytical study of reinforced concrete beams tested under quasi-static and impact loadings. *Appl. Sci.* **2019**, *9*, 2838. [CrossRef]
2. Rampini, M.C.; Zani, G.; Colombo, M.; di Prisco, M. Mechanical behaviour of TRC composites: Experimental and analytical approaches. *Appl. Sci.* **2019**, *9*, 1492. [CrossRef]
3. Poppe, C.; Dorr, D.; Henning, F.; Luise, K. Experimental and numerical investigation of the shear behaviour of infiltrated woven fabrics. *Compos. Part A* **2018**, *114*, 327–337. [CrossRef]
4. Rashidi, A.; Milani, A.S. A multi-step biaxial bias extension test for wrinkling/de-wrinkling characterization of woven fabrics: Towards optimum forming design guidelines. *Mater. Des.* **2018**, *146*, 273–285. [CrossRef]
5. Nosrat Nezami, F.; Gereke, T.; Cherif, C. Active forming manipulation of composite reinforcements for the suppression of forming defects. *Compos. Part A* **2017**, *99*, 94–101. [CrossRef]
6. Harrison, P.; Abdiwi, F.; Guo, Z.; Potluri, P.; Yu, W.R. Characterising the shear–tension coupling and wrinkling behaviour of woven engineering fabrics. *Compos. Part A* **2012**, *43*, 903–914. [CrossRef]
7. Syerko, E.; Comas-Cardona, S.; Binetruy, C. Models for shear properties/behavior of dry fibrous materials at various scales: A review. *Int. J. Mater. Form.* **2015**, *8*, 1–23. [CrossRef]
8. Boisse, P.; Hamila, N.; Guzman-Maldonado, E.; Madeo, A.; Hivet, G.; Dell Isola, F. The bias-extension test for the analysis of in-plane shear properties of textile composite reinforcements and prepregs: A review. *Int. J. Mater. Form.* **2017**, *10*, 473–492. [CrossRef]
9. Cao, J.; Akkerman, R.; Boisse, P.; Chen, J.; Cheng, H.S.; de Graaf, E.F.; Gorczyca, J.L.; Harrison, P.; Hivet, G.; Launay, J.; et al. Characterization of mechanical behavior of woven fabrics: Experimental methods and benchmark results. *Compos. Part A* **2008**, *39*, 1037–1053. [CrossRef]
10. Boisse, P.; Hamila, N.; Vidal-Sallé, E.; Dumont, F. Simulation of wrinkling during textile composite reinforcement forming. Influence of tensile, in-plane shear and bending stiffnesses. *Compos. Sci. Techcol.* **2011**, *71*, 683–692. [CrossRef]
11. Komeili, M.; Milani, A.S. On effect of shear-tension coupling in forming simulation of woven fabric reinforcements. *Compos. Part B* **2016**, *99*, 17–29. [CrossRef]
12. Zhang, W.Z.; Bostanabad, R.; Liang, B.; Su, X.M.; Zeng, D.; Bessa, M.A.; Wang, Y.C.; Chen, W.; Cao, J. A numerical Bayesian-calibrated characterization method for multiscale prepreg preforming simulations with tension-shear coupling. *Compos. Sci. Techcol.* **2019**, *170*, 15–24. [CrossRef]
13. Robitaille, F.; Clayton, B.R.; Long, A.C.; Souter, B.J.; Rudd, C.D. Geometric modelling of industrial preforms: Woven and braided textiles. *Part L J. Mater. Des. Appl.* **1999**, *213*, 69–83. [CrossRef]
14. Long, A.C.; Rudd, C.D.; Blagdon, M.; Smith, P. Characterizing the processing and performance of aligned reinforcements during preform manufacture. *Compos. Part A* **1996**, *27*, 247–253. [CrossRef]
15. King, M.J.; Jearanaisilawong, P.; Socrate, S. A continuum constitutive model for the mechanical behavior of woven fabrics. *Int. J. Solids Struct.* **2005**, *42*, 3867–3896. [CrossRef]
16. Peng, X.Q.; Cao, J. A continuum mechanics-based non-orthogonal constitutive model for woven composite fabrics. *Compos. Part A* **2005**, *36*, 859–874. [CrossRef]
17. Gong, Y.; Yan, D.X.; Yao, Y.; Wei, R.; Hu, H.L.; Xu, P.; Peng, X.Q. An anisotropic hyperelastic constitutive model with tension–shear coupling for woven composite reinforcements. *Int. J. Appl. Mech.* **2017**, *9*, 1750083. [CrossRef]
18. Lomov, S.V.; Verpoest, I. Model of shear of woven fabric and parametric description of shear resistance of glass woven reinforcements. *Compos. Sci. Techcol.* **2006**, *66*, 919–933. [CrossRef]
19. Zhu, B.; Yu, T.X.; Teng, J.; Tao, X.M. Theoretical modeling of large shear deformation and wrinkling of plain woven composite. *J. Compos. Mater.* **2009**, *43*, 125–138. [CrossRef]
20. Erol, O.; Powers, B.M.; Keefe, M. A macroscopic material model for woven fabrics based on mesoscopic sawtooth unit cell. *Compos. Struct.* **2017**, *180*, 531–541. [CrossRef]

21. Nasri, M.; Garnier, C.; Abbassi, F.; Labanieh, A.R.; Dalverny, O.; Zghal, A. Hybrid approach for woven fabric modelling based on discrete hypoelastic behaviour and experimental validation. *Compos. Struct.* **2019**, *209*, 992–1004. [CrossRef]

22. Nosrat-Nezami, F.; Gereke, T.; Eberdt, C.; Cherif, C. Characterisation of the shear–tension coupling of carbon-fibre fabric under controlled membrane tensions for precise simulative predictions of industrial preforming processes. *Compos. Part A* **2014**, *67*, 131–139. [CrossRef]

23. Najjar, W.; Pupin, C.; Legrand, X.; Boude, S.; Soulat, D.; Dal Santo, P. Analysis of frictional behaviour of carbon dry woven reinforcement. *J. Reinf. Plast. Compos.* **2014**, *33*, 1037–1047. [CrossRef]

24. Allaoui, S.; Hivet, G.; Wendling, A.; Ouagne, P.; Soulat, D. Influence of the dry woven fabrics meso-structure on fabric/fabric contact behavior. *J. Compos. Mater.* **2012**, *46*, 627–639. [CrossRef]

25. Ivanov, D.S.; Lomov, S.V. Compaction behaviour of dense sheared woven preforms: Experimental observations and analytical predictions. *Compos. Part A* **2014**, *64*, 167–176. [CrossRef]